Acta Crystallographica Section D
Biological Crystallography
ISSN 0907-4449

Xenon derivatization of halide-soaked protein crystals

Santosh Panjikar and Paul A. Tucker*

EMBL Hamburg Outstation, c/o DESY, Notkestrasse 85, D22603, Hamburg, Germany

Correspondence e-mail: tucker@embl-hamburg.de

Received 22 February 2002
Accepted 19 June 2002

PDB References: model Br-O-Xe-W0.80, 1l0z; model Br-G1-Xe-W0.80, 1l1g.

Crystals of porcine pancreatic elastase can be derived by soaking in high-molarity bromide solutions. These crystals, either in a glycerol-based cryoprotectant solution or in paraffin oil, can be subsequently pressurized under a xenon atmosphere to incorporate xenon. When paraffin oil is used, a larger number of bromide ions are observed on the protein surface. Intensity data collected to lower energy than the bromine absorption edge can be used to determine the xenon position and the resultant phase information can be used to determine the bromine substructure from data collected to higher energy than the bromine absorption edge. The method would appear to have general applicability where large substructures need to be determined.

1. Introduction

The traditional and still popular means of determining the phase of the structure factor of Bragg reflections from a macromolecular crystal has been by the multiple isomorphous replacement (MIR) method or variations of this method that employ the anomalous signal of the derivative (*e.g.* MIRAS and SIRAS). These methods depend not only on the derivative binding but also require that, when bound, the derivative crystal is isomorphous with the native. A practical method has been reported (Boggon & Shapiro, 2000) involving native PAGE analysis that provides some preliminary information on whether or not a derivative compound has bound. The isomorphism, however, can only be tested by X-ray diffraction experiments. Only when xenon or krypton are used as derivatives is there a high probability that – if they bind – the derivative crystal will be isomorphous with the native. This is because the noble gases are expected to bind in (often hydrophobic) cavities/depressions and thus have less likelihood of disrupting or altering crystal contacts.

In recent years, developments in methods of experimental phase determination have been dominated by techniques exploiting the anomalous signal of various elements, in no small part driven by the relative ease with which selenomethionine-containing crystals can be grown and the fact that the selenium absorption edge is easily accessible on modern synchrotron beamlines. These techniques include the traditional MAD experiment at three or more wavelengths (Hendrickson, 1991) as well as, increasingly, SAD experiments where only a single wavelength is used to measure precise anomalous differences at the peak energy. The relative efficacy of these alternatives is still a matter for debate (Rice *et al.*, 2000), but there are increasingly more successes for the SAD technique, especially when highly redundant data sets are

Table 1
Data-collection statistics.

Values in parentheses are for the last resolution shell.

Crystal treatment	Crystal cryoprotected with oil and pressurized under Xe	1 *M* NaBr followed by transfer to oil, then pressurized under Xe	1 *M* NaBr followed by transfer to oil	1 *M* NaBr followed by dipping in 22% glycerol; subsequently pressurized under Xe		Dipped in a 1:1 mixture of 1 *M* NaBr + 100% glycerol; subsequently pressurized under Xe		Dipped in a 1:1 mixture of 1 *M* NaBr + 100% glycerol	Native using oil
Data set	O-Xe-W0.98	Br-O-Xe-W0.80	Br-O-W0.85	Br-G-Xe-W0.80	Br-G-Xe-W0.93	Br-G1-Xe-W0.80	Br-G1-Xe-W0.93	Br-G-W0.80	W0.80
Xe pressure/time	4 MPa/1 min	4 MPa/1 min	—	4 MPa/1 min	4 MPa/1 min	4 MPa/1 min	4 MPa/1 min	—	—
Beamline	BW7A	X13	X11	X13	BW7A	X13	BW7A	X13	X13
Rotation range (°)	180 + 180 (low res.)	360 + 360 (low res.)	360	360	360	360 + 360 (low res.)	360	180	90
Total collection time (h)	8	4	15	11	9	12	11	2	3
Wavelength (Å)	0.980	0.8020	0.85	0.8020	0.918	0.8020	0.918	0.8020	0.80
Crystal-to-detector distance (mm)	45	130	120	100	80	100	80	130	100
Space group	$P2_12_12_1$	$P2_12_12_1$	$P2_12_12_1$	$P2_12_12_1$	$P2_12_12_1$	$P2_12_12_1$	$P2_12_12_1$	$P2_12_12_1$	$P2_12_12_1$
Unit-cell parameters									
a	49.78	49.50	50.23	50.35	50.28	50.29	50.35	50.30	49.92
b	57.30	57.70	57.87	57.87	57.70	57.71	57.74	57.90	57.33
c	73.90	73.60	74.49	74.30	74.11	74.13	74.21	74.52	73.95
Resolution range of last shell (Å)	1.06–1.04	1.53–1.50	1.58–1.55	1.53–1.50	1.27–1.25	1.22–1.20	1.22–1.20	1.53–1.50	1.68–1.65
$\langle I/\sigma(I)\rangle$	33 (3)	34 (10)	23 (18)	10 (4)	19 (4)	19 (8)	48 (4)	30 (7)	16 (7)
Completeness	100 (99)	99 (100)	100 (100)	95 (85)	100 (100)	99 (100)	99 (98)	100 (100)	99 (100)
Mosaicity	0.74	0.9	0.34	1.3	0.9	0.20	0.18	0.35	0.62
No. of observations	729921	598060	480463	361575	830692	1017166	985714	222684	100434
No. of unique reflections	101230	34498	35415	29508	53669	66284	67054	35398	26180
Redundancy	7.2 (6.4)	17.3 (11.3)	13.6 (13.5)	12.3 (9.4)	15.5 (12.5)	15.4 (10.0)	14.7 (14.5)	6.3 (5.9)	3.8 (3.8)
$R_{\rm r.i.m.}$† (%)	6.2	4.5	6.4	6.4	5.1	7.7	4.7	4.0	7.5
$R_{\rm p.i.m.}$‡ (%)	2.0	0.9	1.8	1.7	1.1	1.8	1.2	1.6	3.7
$R_{\rm anom}$§ (%)	1.9	2.7	4.0	2.2	1.7	3.3	1.6	2.4	—
$R_{\rm merge}$¶ (%)	5.8 (20.1)	4.4 (18.0)	6.1 (11.1)	6.2 (14.5)	5.0 (59.8)	7.6 (45.7)	4.5 (59.2)	3.7 (21.0)	7.0 (19.8)

† $R_{\rm r.i.m.}$ is the redundancy-independent merging R factor (Weiss & Hilgenfeld, 1997), which is identical to the $R_{\rm meas}$ of Diederichs & Karplus (1997*a*,*b*). $R_{\rm r.i.m.} = \sum_{hkl}(N/N-1)^{1/2}\sum_i |I_i(hkl) - \overline{I(hkl)}|/\sum_{hkl}\sum_i I_i(hkl)$, with N being the number of times a given reflection has been observed. ‡ $R_{\rm p.i.m.}$ is the precision-indicating merging R factor (Weiss & Hilgenfeld, 1997; Weiss, 2001). $R_{\rm p.i.m.} = \sum_{hkl}(1/N-1)^{1/2}\sum_i |I_i(hkl) - \overline{I(hkl)}|/\sum_{hkl}\sum_i I_i(hkl)$. § $R_{\rm anom} = \sum_{hkl}|I(hkl) - I(\overline{hkl})|/\sum_{hkl}\overline{I(hkl)}$. ¶ $R_{\rm merge} = \sum_{hkl}\sum_i |I_i(hkl) - \overline{I(hkl)}|/\sum_{hkl}\sum_i I_i(hkl)$ (Stout & Jensen, 1968).

measured. The practical repertoire of phasing procedures has, however, continued to grow with, for example, the use of xenon as a derivative (Schiltz *et al.*, 1995), the use of halide soaks to produce derivatives (Dauter & Adamiak, 2001; Dauter & Dauter, 1999) or the use of longer wavelengths to utilize the anomalous signal from S atoms in crystals of native proteins (Hendrickson & Teeter, 1981; Dauter *et al.*, 1999). Of some interest to us are combinations of these newer techniques and in particular the combined use of xenon and bromide ions, with or without utilization of energies higher and lower than the bromine absorption edge. The number of possible bromide-ion interaction sites is typically large, which can result in a bromide substructure that is difficult to determine. We wished to investigate the use of the less numerous xenon sites in determining the bromide substructure by utilizing two wavelengths: one at lower energy than the bromine absorption edge, where only the xenon has an appreciable anomalous signal, and one at higher energy than the bromine absorption edge, where the f'' values of both elements are roughly the same.

2. Materials and methods

Porcine pancreatic elastase (PPE) was crystallized as described previously (Shotton *et al.*, 1968). Crystals of PPE of approximate dimensions 0.4 × 0.2 × 0.2 mm were mounted in cryoloops (Teng, 1990) from Hampton Research and treated as described below prior to flash-cooling in liquid nitrogen.

2.1. Bromide and xenon derivatization

Three different protocols were used as follows.

Protocol 1. Crystals were removed from the mother liquor and immediately dipped for 20 s into 1 *M* NaBr solution. They were then transferred into a cryoprotectant solution consisting of 22%(*v*/*v*) glycerol in distilled water. The cryoloop was then placed inside a xenon pressure cell (http://www.hamptonresearch.com/hrproducts/4791.html) in which a vial of the cryoprotectant had been previously placed to avoid the crystal drying out. The cell was pressurized to 4 MPa xenon for 1 min and the pressure released slowly over 20–30 s. The sample was then flash-cooled in liquid nitrogen in less

than 10 s and stored at liquid-nitrogen temperature (data sets Br-G-Xe-W0.80 and Br-G-Xe-W0.93).

Protocol 2. Crystals were similarly removed from the mother liquor and immediately dipped for 20 s into a 1 *M* NaBr solution. They were then transferred to 200 µl of dry paraffin oil to remove the aqueous layer around the crystals. They were then either flash-cooled directly (data set Br-O-W0.85) or transferred to the xenon pressure cell, where they were pressurized to 4 MPa for just under 1 min before releasing the pressure slowly and flash-cooling in liquid nitrogen (data set Br-O-Xe-W0.80). Crystals derivatized with xenon alone (data set O-Xe-W0.98) were produced by transfer directly to dry paraffin oil prior to derivatization and flash-cooling.

Protocol 3. Crystals were transferred to a 1:1 mixture of glycerol (100%) and 1 *M* NaBr for 20 s and were either directly flash-cooled (data set Br-G-W0.80) or transferred to the xenon pressure cell and pressurized using the same protocol as described above (data sets Br-G1-Xe-W0.80 and Br-G1-Xe-W0.93).

2.2. Data collection

Data were measured on the derivatized crystals at different wavelengths on different beamlines (BW7A, X13 and X11), essentially as a consequence of beamline availability but with the requirement that some crystals give data sets obtained to both lower and higher energy than the bromine absorption edge (Br-G-Xe-W0.80/Br-G-Xe-W0.93, Br-G1-Xe-W0.80/Br-G1-Xe-W0.93 and O-Xe-W0.98/Br-O-W0.85). The crystals were retrieved from and restored to the various beamlines using a conventional arc (similar to that described by Mancia *et al.*, 1995). Each data set was processed with the *HKL* package (Otwinowski & Minor, 1997) but scaled with the *CCP*4 (Collaborative Computational Project, Number 4, 1994) program *SCALA*. Statistics for all data collections are summarized in Table 1. The data sets were all measured with high redundancy to maximize the ratio of $R_{\rm anom}$ to $R_{\rm p.i.m.}$ We have previously found this ratio to be a good indicator of phasing power (Panjikar & Tucker, 2002*b*). For reference, a native data set was measured from a crystal flash-cooled in paraffin oil.

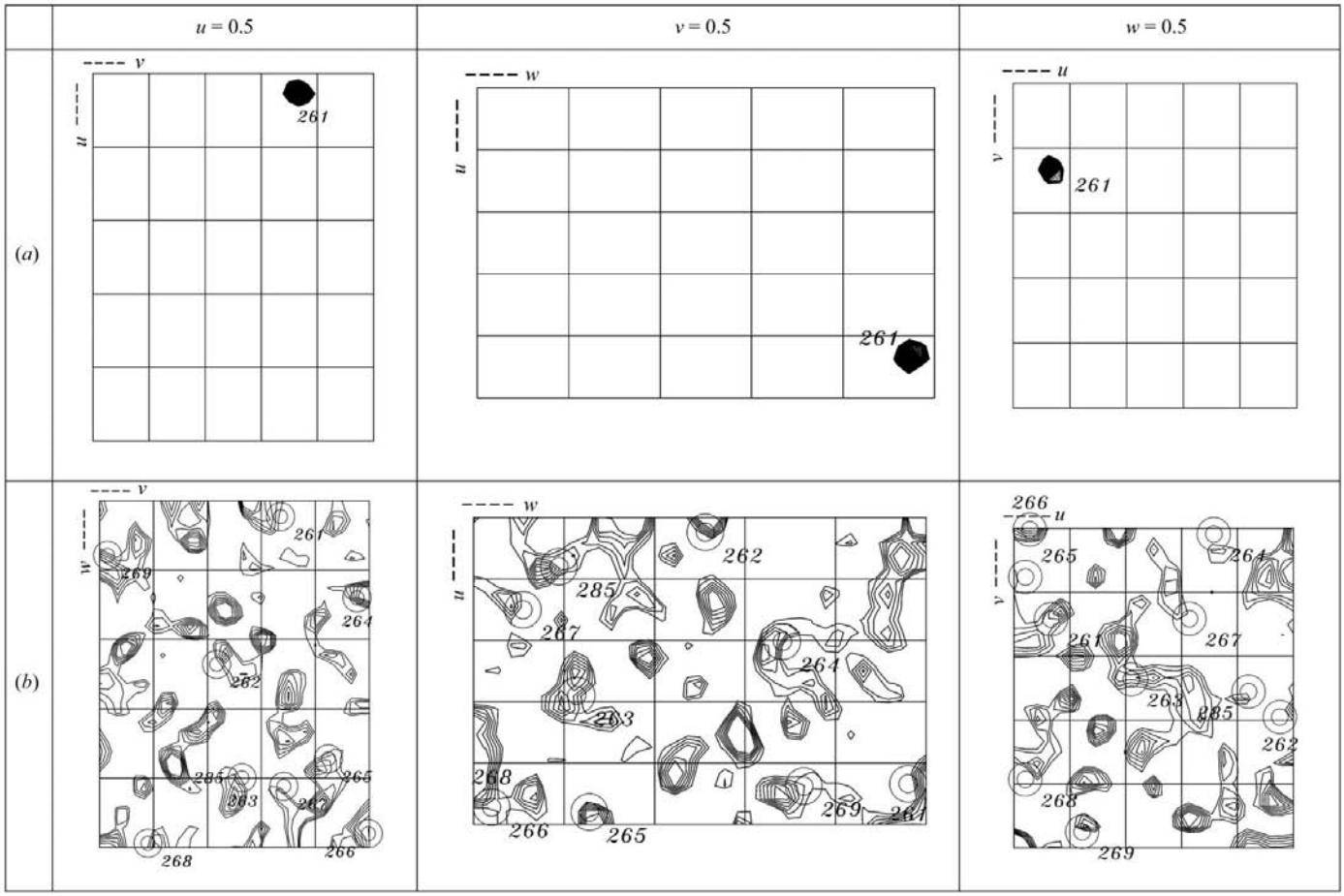

Figure 1
The Harker sections of the anomalous difference Patterson for (*a*) the Br-Xe-G1-W0.93 and (*b*) the Br-Xe-G1-W0.8 data set. The expected vector positions are marked with circles and the xenon (261) and bromide vectors are numbered as in Table 2.

Table 2
Comparison of Br sites from the initial phases, using the common numbering scheme used in the PDB entries.

The occupancy and temperature factor from the heavy-atom refinement are given. Blank spaces show that bromine is not present in this position.

Site No.	*x*	*y*	*z*	Br-O-Xe-W0.80	Br-O-W0.85	Br-G-Xe-W0.80/ Br-G-Xe-W0.92	Br-G1-Xe-W0.80/ Br-G1-Xe-W0.92	Br-G-W0.80
Xe261	0.283	0.429	0.010	1.01/18.6		1.22/21.8	1.17/22.0	
Br262	0.512	0.651	0.124	1.01/14.9	0.63/05.0	0.65/13.0	1.13/16.3	0.86/11.5
Br263	0.352	0.378	0.309	0.85/21.1	0.76/11.7	0.56/13.4	0.79/20.3	0.47/15.4
Br264	0.904	0.500	0.068	0.48/21.9	0.76/19.5	0.21/22.0	0.38/16.4	0.38/26.3
Br265	0.760	0.544	0.189	0.31/11.7	0.32/05.7	0.23/23.8	0.41/22.2	0.26/18.6
Br266	0.261	0.495	0.240	0.47/14.3	0.80/16.6	0.16/10.0	0.38/11.9	0.27/08.5
Br267A	0.407	0.588	0.284	0.33/23.9	0.37/15.8	0.16/12.5	0.34/21.1	0.40/36.0
Br267B	0.417	0.581	0.299	†				
Br268	0.258	0.291	0.254	0.59/21.2	0.55/14.2	0.14/08.6	0.59/65.5‡	0.19/14.5
Br269	0.699	0.246	0.046	0.68/32.8	0.65/23.3		†	0.21/24.6
Br270A	0.320	0.748	0.268	0.43/31.9	0.42/22.1			0.20/14.0
Br270B	0.315	0.732	0.272	†				
Br271	0.857	0.828	0.115	0.72/36.5	0.34/29.5			0.18/20.6
Br272	0.481	0.992	0.170	0.34/35.7	0.27/19			0.23/24.8
Br273	0.715	0.825	0.222	0.27/27.9	0.43/44.3	0.21/48.6		
Br274	0.555	0.281	0.321	0.24/14.6	0.37/12.6			
Br275	0.127	0.195	0.189	0.44/31.6	0.31/13.4			
Br276	0.699	0.780	0.123	0.37/37.6	0.67/70.3			
Br277	0.688	0.255	0.189	0.61/48.5	0.34/29.5			
Br278	0.004	0.748	0.107	0.29/27.5	0.34/35.7			
Br279	0.889	0.414	0.177	0.29/29.5	0.43/29.0			
Br280	0.956	0.874	0.202	0.33/33.2	0.30/22.7			
Br281	0.838	0.652	0.124	0.22/29.7	0.27/04.1			
Br282	0.824	0.509	0.156	0.28/35.8	0.44/28.6			
Br283	0.017	0.979	0.138	0.21/39.3	1.07/30.5			
Br284	0.140	0.875	0.164	0.41/45.6	0.59/38.7			
Br285	0.463	0.377	0.304	0.79/20.8			0.38/21.8	0.21/09.7
Br286	0.338	0.035	0.018	0.22/24.1				
Br287	0.148	0.989	0.176	0.36/40.9				
Br288	0.154	0.214	0.132	0.14/19.4				
Br289	0.628	0.835	0.065	0.23/25.5				
Br290	0.872	0.061	0.091	0.45/57.3				
Br291	0.850	0.104	0.027	0.20/26.8				
Br292	0.878	0.351	0.119	†	0.45/35.5			
Br293	0.412	0.907	0.182	†	0.22/11.5			
Br294	0.501	0.754	0.238	0.35/42.0‡				
Br295	0.803	0.059	0.000		0.27/10.3			
Br296	0.591	0.484	0.244		0.50/28.4			
Br297	−0.002	0.846	0.155		0.24/13.4			
Br298	0.733	0.083	0.052		0.42/12.2			
Br299	0.305	0.921	0.050		0.45/27.5			
Br300	0.984	0.678	0.027		0.43/31.4			

† These atoms appeared in model refinement. ‡ These atoms were subsequently removed when the model was refined.

Table 3
Values of f' and f'' used.

	λ = 0.80 Å		λ = 0.85 Å		λ = 0.93 Å		λ = 0.98 Å	
	f'	f''	f'	f''	f'	f''	f'	f''
Br	−1.0	2.99	−1.7	3.29	−4.0	0.05	−2.46	0.56
Xe	−0.5	2.45	−0.46	2.68	−0.3	3.1	−0.31	3.43

2.3. Location of Xe atoms and bromide ions

To test the efficacy of a procedure that uses data at two wavelengths, the pairs of data sets Br-G-Xe-W0.80/Br-G-Xe-W0.93, Br-G1-Xe-W0.80/Br-G1-Xe-W0.93 and O-Xe-W0.98/Br-O-W0.85 were used. The first two pairs were collected on the same crystal, whereas for the third pair different crystals were used. Data to 2.0 Å were used and the xenon position was located by inspection of Harker sections of an anomalous difference Patterson using the data sets collected to lower energy than the bromine edge (Fig. 1*a* for the Br-Xe-G1-W0.93 data set) or, in the case of the third pair, the data set from the crystal containing xenon only (O-Xe-W0.98). The position and occupancy of the Xe atom were refined using *SHARP* (de La Fortelle & Bricogne, 1996) and SAS phases were calculated and improved by density modification as implemented in *SHARP* [*DM* (Cowtan & Zhang, 1999) and *SOLOMON* (Abrahams & Leslie, 1996)]. For the first two pairs of data sets, anomalous difference Fouriers were generated using the *FFT* (Ten Eyck, 1973) program with the data set to higher energy than the bromine edge and using the xenon-derived SAS phases. This enabled the location of the eight major bromide sites. For the third pair, the anomalous difference Fourier using the bromide-only data set (Br-O-W0.85) was calculated using the SAS phases derived from the xenon-only data set (O-Xe-W0.98). This enabled 24 of the bromide sites to be identified; the remaining sites were located from residual maps calculated using Fourier coefficients derived from gradients of the log-likelihood function, as described by La Fortelle & Bricogne (1997).

As an alternative *AutoSHARP* was also used *a priori* to locate and refine the heavy-atom sites (Table 2) for the Br-O-Xe-W0.80 data. *AutoSHARP* found seven of the 32 bromide/xenon sites in the first round and a further 11 in the second round. After optimization of solvent content, the automated model-building procedure terminated with a correlation coefficient marginally lower than 70%; however, the phase set was good enough to autobuild the model.

2.4. Phasing procedures and model building

With *SHARP*, SAS protocols were used for the Br-O-Xe-W0.80, Br-O-W0.85, Br-G-W0.80, Br-G1-Xe-W0.93 and O-Xe-W0.98 data sets, MAD protocols for the Br-G-Xe-W0.80/Br-G-Xe-W0.93 and Br-G1-Xe-W0.80/Br-G1-Xe-W0.93 pairs and a MIRAS protocol for the O-Xe-W0.98/Br-O-W0.85 pair. The full complement of bromide sites (Table 2) was located by use

Table 4
Phasing statistics at 2.0 Å.

	SAS	SAS	MAD	MAD	SAS	SAS	SAS	MIRAS
	Br-O-Xe-W0.80	Br-O-W0.85	Br-G-Xe-W0.80/ Br-G-Xe-W0.93	Br-G1-Xe-W0.80/ Br-G1-Xe-W0.93	Br-G-W0.80	Br-G1-Xe-W0.93	O-Xe-W0.98	O-Xe-W0.98, Br-O-W0.85
No. of Xe sites	1	—	1	1	—	1	1	1
No. of Br sites	31	32	7	9	13	—	—	32
SHARP FOM	0.57	0.52	0.64	0.65	0.42	0.41	0.33	0.60
SHARP correlation coefficient	0.55	0.44	0.48	0.47	0.42	0.37	0.37	0.54
SHARP ($\Delta\varphi$)	62.75	68.63	63.67	63.31	68.86	70.20	70.80	54.15
SHARP density-modified FOM	0.91	0.89	0.87	0.91	0.84	0.84	0.83	0.91
SHARP density-modified CC	0.76	0.71	0.73	0.75	0.67	0.52	0.49	0.78
SHARP density-modified $\Delta\varphi$	48.87	53.67	52.45	50.75	56.01	62.04	64.09	43.67
SHARP-ARP/wARP residues/building cycles	224/9	210/9	221/9	219/9	194/9	—	—	220/9

Table 5
Refinement statistics from *SHELXL*.

	Br-O-Xe-W0.80	Br-G1-Xe-W0.80
Resolution range (Å)	35–1.5	35–1.5
R factor (%)	16.6	17.3
$R_{\rm free}$ (%)	20.9	21.5
No. of protein atoms	1832	1832
Main-chain average *B* factor (Å^2)	15.1	14.2
Side-chain average *B* factor (Å^2)	17.3	16.7
No. of water atoms	305	216
Water average *B* factor (Å^2)	29.6	28.9
No. of bromide ions	34	8
Bromide average *B* factor (Å^2)	27.6	26.5
No. of Xe atoms	1	1
B factor of Xe atom (Å^2)	18.5	15.8
No. of Na atoms	1	1
B factor of Na atom (Å^2)	11.7	13.3
No. of glycerol molecules	0	1
B factor of glycerol molecule (Å^2)	—	30.0
No. of sulfate ions	0	1
B factor of sulfate ions (Å^2)	—	24.0
R.m.s. deviation from ideal values†		
Bond lengths (Å)	0.009	0.010
Bond angles (°)	2.13	2.18
Residue distribution in Ramachandran plot‡		
Most favourable region (%)	88.3	87.9
Allowed region (%)	11.7	12.1

† Engh & Huber (1991). ‡ Ramachandran & Sasisekharan (1968).

of the residual maps in *SHARP*. In the refinements, f' and f'' of bromine and xenon were not refined and the theoretical values used for the different wavelengths are given in Table 3.

A PPE model (PDB code 1qnj) was rebuilt and rerefined using *ARP* (Lamzin & Wilson, 1993) and *REFMAC* (Murshudov *et al.*, 1997). Refinements against the W0.8 data set were made at 2.0 Å. The *R* factor and $R_{\rm free}$ were 18 and 22%. Phase errors and map correlation coefficients (using $2mF_{\rm obs} - DF_{\rm calc}$, $\varphi_{\rm calc}$) before and after density modification with the refined structure were calculated for each of the phasing procedures using *SFTOOLS* (Collaborative Compuatational Project, Number 4, 1994) and are given in Table 4. It should be noted that the map correlation coefficients are against the 'native' structure, whereas the determined phases are for the derivatized models. The native data set was not used in the phasing procedures. Finally, the quality of the phases (at 2 Å) was checked by the ability to automatically build the protein model using *ARP*/*wARP* (Perrakis *et al.*, 1999); the number of correctly built residues (out of 240) in a given number of building cycles is also listed in Table 4. In each case, if the phases were extended by density modification to 1.5 Å the entire structure could be autobuilt within 3–4 building cycles.

2.5. Refinement of the bromide/solvent models

Because of the different number of bromide sites observed between the glycerol and oil-treated crystals, two of the bromide-containing structures were refined using *SHELXL*97 to establish the major differences. PDB entry 1qnj was used as starting model for the data sets Br-O-XeW-0.8 and Br-G1-Xe-W0.8. 20 cycles of rigid-body refinement were carried out to 2.5 Å resolution to ensure that the model was correctly placed in the unit cell. Using conjugate-gradient least-squares (CGLS) refinement, the resolution was increased by 0.02 Å per step from 2.5 to 1.5 Å in 50 cycles. After these refinement steps, side chains were (re)placed correctly using the electron density ($2mF_{\rm obs} - DF_{\rm calc}$) and difference density ($mF_{\rm obs} - DF_{\rm calc}$) maps. Subsequently, each round of refinement consisted of 20 CGLS cycles. After the first three rounds, peaks from a difference Fourier synthesis calculated by *SHELXL* were compared with an anomalous difference Fourier map to check the correct placement of the bromide ions, the Xe atom and the sodium ion in the model. Subsequently, the occupancies of these heavy atoms were refined, the refined occupancies were fixed, isotropic *B*-factor refinement was performed and finally the atoms were allowed to refine with anisotropic temperature factors. After subsequent refinement steps, difference Fourier peaks ($>5\sigma$) were added to the model as water molecules subject to reasonable contact distances and reasonably shaped electron density.

The Br-O-XeW-0.8 data provides a model where the sulfate ion (in 1qnj) is replaced by a bromide ion. The Br-G1-Xe-W0.8 data provides a model which contains one glycerol molecule (at a protein–protein contact) and one sulfate ion. The refinements are summarized in Table 5.

3. Results and discussion

Soaking in NaBr followed by removal of the aqueous layer around the crystal in dry paraffin oil (data sets Br-O-Xe-W0.80 and Br-O-W0.85) results in crystals with far more bromide sites (Table 2) than when glycerol is used as a cryoprotectant. The probable factors contributing to this are either the absence of a back-soak (*e.g.* Br-G-Xe-W0.80) or the reduced NaBr concentration (*e.g.* Br-G1-Xe-W0.80), or even the competition between bromide and glycerol to 'solvate' the protein. The larger number of sites results in improved phasing, as judged by the mean phase error after density modification (compare Br-O-W0.85 and Br-G-W0.8 in Table 4), a presumed consequence of the larger $R_{\rm anom}/R_{\rm p.i.m.}$ ratio, resulting almost entirely from a larger value of $R_{\rm anom}$ (see Table 1). Of course, f'' is around 10% higher for the first data set, but the effect of this is not dominant. This suggests that there is a clear advantage of using oil as a 'cryoprotectant' when using halide soaks. We have previously reported the advantage of using oil when xenon derivatization is required (Panjikar & Tucker, 2002*a*). The better phasing obtained for the Br-O-Xe-W0.80 data relative to the Br-O-W0.85 data does not result so much from the addition of xenon, but from the better $R_{\rm anom}/R_{\rm p.i.m.}$ ratio of the former set. This is more highly redundant because a low-resolution data set was measured; consequently, $R_{\rm p.i.m.}$ is lower and the data is more complete at low resolution. In the 20.0–4.0 Å resolution range, the values were 99.8% for the Br-O-Xe-W0.80 data set compared with 95.7% for the Br-O-W0.85 data set. The wavelength difference in this case is expected to result in a larger $R_{\rm anom}$ for the former rather than the latter data set (Table 3), other things being equal.

The resultant phases determined using Xe only in an SAS protocol (data sets Br-G1-Xe-W0.93 and O-Xe-W0.98) are generally not good enough to autobuild the model at 2.0 Å, but they are certainly adequate to locate Br atoms in bromide-soaked crystals. Using such two-wavelength data sets gives mean phase errors that are sufficiently good to

Table 6
Comparison of bromide–protein/water contacts.

* indicates atoms from a symmetry-related molecule.

		Br-O-Xe-W0.80	Br-G1-Xe-W0.80			Br-O-Xe-W0.80	Br-G1-Xe-W0.80
Br262	Pro13 N	3.66	3.58	Br275	Gly23 N	3.48	—
	Wat394 OW0	3.28	3.38		Br288	3.28	—
	Ser14 N	3.42	3.41		Wat567 OW0	2.60	—
	Ser14 OG	3.13	3.09		Wat 520 OW0	3.63	—
	Wat398 OW0	4.00	—	Br276	Ser107 N	3.57	—
	Wat368 OW0	3.03	3.21		Wat537 OW0	2.40	—
	Wat312 OW0	3.85	3.93	Br277	Asn240 ND2	2.80	—
Br263	Ala228 CA	3.93	—	Br278	Arg9 NH2	3.79	—
	Arg136 NH1	3.62*	3.91*		Wat396 OW0	3.12	—
	Wat468 OW0	2.98	—		Asn61 ND2	3.20	—
	Arg225 NH1	3.35	3.29		Wat427 OW0	2.21	—
	Arg225 NH2	3.53	3.54	Br279	Ser160 OG	3.82	—
Br264	Wat432 OW0	3.61	—		Ser162 N	3.56	—
	Wat633 OW0	—	3.43		Ser162 OG	2.42	—
	Arg218 NE	—	3.75		Ser161 OG	3.97	—
	Ser102 N	3.35	3.46	Br280	Wat548 OW0	3.90	—
	Wat419 OW0	3.73	3.80		Wat577 OW0	3.93	—
Br265	Gln37 N	3.41	3.27		Gln143 OE1	3.28	—
	Gln37 NE2	—	3.94		Asn63 OD1	3.34	—
	Wat508 OW0	3.02	—	Br281	Leu105 N	3.15	—
Br266	Wat307 OW0	3.01	3.05		Gln37 OE1	3.49	—
	Leu121 N	3.30	3.26	Br282	Arg218 NH2	3.48	—
	Wat331 OW0	3.04	2.82		Ser102 OG	3.05	—
	Wat371 OW0	3.19	—		Asn38 OD1	3.74	—
Br267A	Wat531 OW0	3.43	—	Br283	Trp26 O	3.92	—
	Wat534 OW0	3.84	—		His28 N	3.04	—
	Arg116 N	3.88	—		Wat412 OW0	2.79	—
	His203 NE2	3.76	—	Br284	Asn65 N	3.63	—
Br267B	Wat531 OW0	3.41	—		Wat521 OW0	2.48	—
	Wat534 OW0	2.99	—		Gln64 N	3.76	—
	Wat639 OW0	—	3.76		Gln64 O	3.81	—
	Wat267 OW0	—	2.17	Br285	Ser231 N	3.32	3.34
	Arg116 NH1	—	3.72		Ser1231 N	3.32	—
	Arg116 N	3.12	3.17		Ser1231 OG	3.16	—
	Thr119 OG1	—	3.69		Ser231 OG	—	3.67
Br268	Ser171 N	3.59	—		Ala228 O	3.73	3.54
	Wat435 OW0	3.14	—		Ile230 N	3.42	3.42
	Asn170 N	3.90	—		Wat382 OW0	3.51	3.40
	Wat381 OW0	3.54	—		Ser227 O	3.93	3.95
	Wat535 OW0	3.62	—	Br286	Gln101 OE1	3.09	—
Br269	Wat478 OW0	3.41	—		Wat402 OW0	2.52	—
	Ile77 N	3.29	3.29		Gly73 N	2.67	—
	Ile77 O	3.96	3.92		Wat505 OW0	2.24	—
	Wat434 OW0	3.12	3.13	Br287	Trp26 N	3.12	—
Br270A	Gly198 N	3.15	—		Trp26 O	3.79	—
	Asn235 O	3.36*	—	Br288	Lys169 NZ	2.83	—
	Ser239 OG	2.51*	—		Wat452 OW0	2.81	—
	Leu195 CG	3.66	—		Ser166 O	3.56	—
Br270B	Gly198 N	3.31	—		Wat369 OW0	2.22	—
	Ser239 OG	3.20*	—		Br275	3.28	—
	Val196 C	3.99	—		Wat395 OW0	3.25	—
	Asn197 N	3.49	—	Br289	Gly3 N	3.93	—
	Wat438 OW0	3.72	—		Wat303 OW0	3.32	—
Br271	Thr144 N	3.62	—		Ser107 OG	3.27	—
	Thr144 OG1	3.67	—		Wat449 OW0	2.02	—
	Gln143 N	3.25	—		Wat370 OW0	2.70	—
	Gln146 NE2	3.91	—		Asn10 ND2	3.35	—
	Wat487 OW0	3.84	—		Wat565 OW0	3.61	—
Br272	Wat375 OW0	3.37	—	Br290	Wat440 OW0	3.29	—
	Wat499 OW0	3.21	—		Wat388 OW0	3.90	—
	Ala117 N	3.14	—		Gly186 N	3.84	—
	Wat562 OW0	3.79	—		Wat507 OW0	3.25	—
Br273	Asn170 O	3.72	—	Br291	Wat423 OW0	3.86	—
	Ser171 N	3.56	—		Gly186 N	3.25	—
	Arg225 NH2	3.28	—		His45 NE2	3.80	—
	Wat598 OW0	2.43	—		Ser188 OG	2.64	—
	Wat489 OW0	2.64	—				

Table 6 (continued)

		Br-O-Xe-W0.80	Br-G1-Xe-W0.80			Br-O-Xe-W0.80	Br-G1-Xe-W0.80
Br274	Asn235 ND2	3.18	—	Br292	Ile77 O	3.33	—
	Wat321 OW0	3.41	—		Wat434 OW0	3.38	—
	Wat512 OW0	3.33	—		Wat559 OW0	3.82	—
					Val79 N	3.07	—
					Wat594 OW0	2.97	—
					Wat431 OW0	3.12	—
				Br293	Ser231 OG	3.54	—
					Asn234 ND2	2.76	—

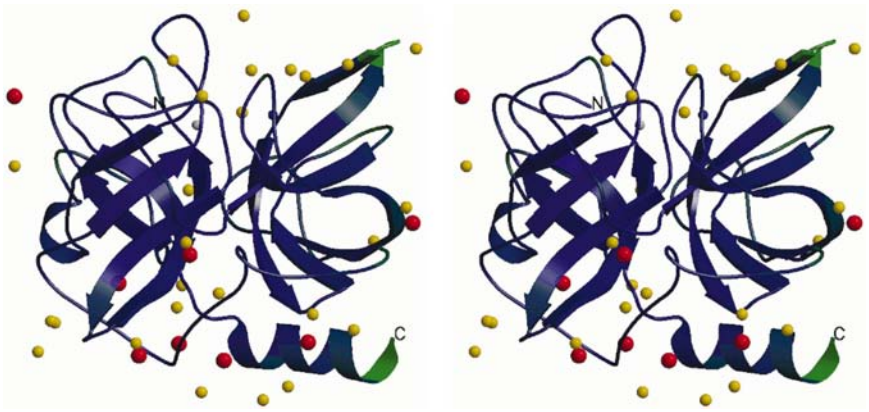

Figure 2
Stereo cartoon of PPE with regions coloured from blue to green according to increasing main-chain temperature factor. Bromide ions common to both glycerol and oil cryoprotection conditions are shown in red; those bromide positions found only with the oil treatment are shown in yellow. The Xe atom is coloured grey, whilst the sodium ion is deep blue.

allow automatic model building at 2 Å, despite the fact that the individual $R_{\rm anom}/R_{\rm p.i.m.}$ ratios of the individual data sets are not as good as when oil was used for cryoprotection. It is also possible to use the same strategy when different crystals are used. For example, the data set O-Xe-W0.98 can yield phases that locate 24 sites in the Br-O-W0.85 data set (these phases also locate 22 bromide sites from the Br-O-Xe-W0.80 data). Both data sets when used together in a MIRAS phasing strategy yield a phase set (Table 4) which after density modification allows autobuilding in *ARP*/*wARP* at 2.0 Å.

It would appear that there is a viable phasing strategy that uses the differential differences in f'' between Br and Xe across the bromine absorption edge to determine the bromide substructure from SAS phases from the fewer, and therefore more easily determined, xenon sites (Fig. 1). To lower energy than the bromine absorption edge, the anomalous difference Patterson is easier to interpret than the isomorphous difference Patterson because the latter contains vectors from both bromine and xenon. The generality of such a strategy will depend on the crystal surviving the two treatments, although a similar strategy for solving selenium substructures (using the xenon derivative to higher and lower energy than the selenium absorption edge) in selenomethionine-containing crystals would require only xenon pressurization. In our limited experience, xenon pressurization does not destroy crystals, although we have observed phase changes resulting from pressurization. We have preferred to use 4 MPa for short times rather than lower pressures (0.5–1 MPa) for longer times, but have no indication that the former protocol has specific advantages in terms of xenon occupancy. Rather, the problem is that often we see no xenon binding, but as yet we have too few examples to give statistics. We would expect the bromide soaks to be far more damaging since, depending on crystallization conditions, there might be a large change in ionic strength that many protein crystals would not survive.

It is interesting to note that the location and number of bromide ions is not reproducible from crystal to crystal. For aqueous solutions this is perhaps not so surprising since the time of soaks are not totally identical, but only the first seven bromide sites are totally reproducible. In oil the situation is rather better, with the first 23 of the 31/32 sites reproducibly observed (Table 2), but again the initial soak conditions are necessarily difficult to reproduce given slight changes in concentration of NaBr, difference in crystal sizes and actual time taken to remove the mother liquor surrounding the crystal. In Table 2, both refined occupancy and temperature factor are given because, although a strong correlation between these parameters is expected, there is no reason to expect that all bromides will have the same temperature factor.

The top seven sites found in all conditions are either located between molecules close to crystal contacts between molecules or occupy appreciable depressions in the protein surface. The positions of the bromide ions are shown in Fig. 2. They are strongly hydrogen bonded (<3.4 Å) to one or more water molecules as well as to predominantly main-chain atoms (see Table 6).

4. Conclusions

We show that crystals of porcine pancreatic elastase can be derivatized by soaking in high-molarity bromide solutions and that these crystals, either in a glycerol-based cryoprotectant solution or in paraffin oil, can be subsequently pressurized under a xenon atmosphere to incorporate xenon. We observe that when paraffin oil is used a larger number of bromide ions are observed on the protein surface. We believe this occurs not only because the glycerol cryoprotection is in some sense a back soak, but also because in glycerol the solvent structure around the protein is more disordered. We show that intensity data collected to lower energy than the bromine absorption edge can be used to determine the xenon position and the resultant phase information can be used to determine the

bromine substructure from data collected to higher energy than the bromine absorption edge. The method would appear to have general applicability where large substructures need to be determined.

This work was performed as part of the EXMAD project with support from the European Union (Contract Number HPRI-CT-1999-50015).

References

Abrahams, J. P. & Leslie, A. G. W. (1996). *Acta Cryst.* D**52**, 30–42.
Boggon, T. J. & Shapiro, L. (2000). *Structure Fold. Des.* **8**, R143–R149.
Collaborative Computational Project, Number 4 (1994). *Acta Cryst.* D**50**, 760–763.
Cowtan, K. D. & Zhang, K. Y. (1999). *Prog. Biophys. Mol. Biol.* **72**, 245–270.
Dauter, Z. & Adamiak, D. A. (2001). *Acta Cryst.* D**57**, 990–995.
Dauter, Z. & Dauter, M. (1999). *J. Mol. Biol.* **289**, 93–101.
Dauter, Z., Dauter, M., de La Fortelle, E., Bricogne, G. & Sheldrick, G. M. (1999). *J. Mol. Biol.* **289**, 83–92.
Diederichs, K. & Karplus, P. A. (1997*a*). *Nature Struct. Biol.* **4**, 269–275.
Diederichs, K. & Karplus, P. A. (1997*b*). *Nature Struct. Biol.* **4**, 592.
Engh, R. A. & Huber, R. (1991). *Acta Cryst.* A**47**, 392–400.
Hendrickson, W. A. (1991). *Science*, **254**, 51–58.
Hendrickson, W. A. & Teeter, M. M. (1981). *Nature (London)*, **290**, 107–113.
La Fortelle, E. de & Bricogne, G. (1997). *Methods Enzymol.* **276**, 472–494.
Lamzin, V. & Wilson, K. S. (1993). *Acta Cryst.* D**49**, 129–147.
Mancia, F., Oubridge, C., Hellon, C., Woollard,T., Groves, J. & Nagai, K. (1995). *J. Appl. Cryst.* **28**, 224–225.
Murshudov, G. N., Vagin, A. A. & Dodson, E. J. (1997). *Acta Cryst.* D**53**, 240–255.
Otwinowski, Z. & Minor, W. (1997). *Methods Enzymol.* **276**, 307–326.
Panjikar, S. & Tucker, P. A. (2002*a*). *J. Appl. Cryst.* **35**, 117–119.
Panjikar, S. & Tucker, P. A. (2002*b*). *J. Appl. Cryst.* **35**, 261–266.
Perrakis, A., Morris, R. & Lamzin, V. S. (1999). *Nature Struct. Biol.* **6**, 458–463.
Ramachandran, G. N. & Sasisekharan, V. (1968). *Adv. Protein Chem.* **23**, 283–437.
Rice, L. M., Earnest, T. N. & Brunger, A. T. (2000). *Acta Cryst.* D**56**, 1413–1420.
Schiltz, M., Fourme, R., Broutin, I. & Prangé, T. (1995). *Structure*, **3**, 309–316.
Shotton, D. M., Hartley, B. S., Camerman, N., Hofmann, T., Nyburg, S. C. & Rao, L. (1968). *J. Mol. Biol.* **32**, 155–156.
Ten Eyck, L. F. (1973). *Acta Cryst.* A**29**, 183–191.
Teng, T. (1990). *J. Appl. Cryst.* **23**, 387–391.
Weiss, M. S. (2001). *J. Appl. Cryst.* **34**, 130–135.
Weiss, M. S. & Hilgenfeld, R. (1997). *J. Appl. Cryst.* **30**, 203–205.